River Flow 2014 – Schleiss et al. (Eds)

Effect of bed elevation discordance in the main river on the confluence hydrodynamics in 90° straight-channels' confluences

D. Đorđević
Faculty of Civil Engineering, University of Belgrade, Belgrade, Serbia

ABSTRACT: A role of the difference in bed elevations in the main-river (Δz_{MR}) at its entrance to a 90° straight-channels' confluence is studied numerically using a 3D finite-volume model. Three characteristic hydrological scenarios with $D_R = \{0.250, 0.583, 0.750\}$ are analysed in four confluence layouts having $\Delta z_{MR}/h_d \in [0.0, 0.50]$ (where h_d stands for the flow depth in the deeper canal at the confluence). It is found that: 1) a portion of the tributary flow in the bottom layers is entrained by the bed-step, 2) the w-velocity has the same order of magnitude as V_{xy} for $\Delta z_{MR} \geq 0.25 h_d$ and $D_R > 0.5$, 3) the opposite bank is endangered by erosion due to strong upward motion along this bank, 4) additional shear layer develops on the outer side of the distorted $u_{\max}$-core and 5) the presence of bed-step favours bed-load transport both in and far downstream of the confluence.

1 INTRODUCTION

Laboratory experiments in movable bed models of confluences showed that the difference in bed elevations between each of the converging channels and an outgoing channel (Post-Confluence Channel, hereinafter designated as PCC) developed in symmetrical (Y-shaped) confluences (Mosley 1976, Ashmore & Parker 1983) and asymmetrical confluences with junction angles larger than 45° (Best 1988, Weerakoon et al. 1990). The increase in the bed elevation discordance was accompanied with the evolution of a scour hole in the so called Confluence Hydrodynamics Zone (CHZ). Both the scour hole and difference in bed elevations between the channels developed through the continuing interaction between the flow and the movable bed. Bathymetric surveys in alluvial river confluences (Kennedy 1984, Đorđević 2010) confirmed the existence of the two morphological features. Their presence in the confluence adds to an already complex flow pattern in the CHZ caused by the collision of the combining flows.

Considerable efforts were made to study the role of bed elevation discordance between the tributary and main-river channels during last 25 years. They included laboratory (Best & Roy 1991, Gaudet & Roy 1995, Bradbrook et al. 1998, Biron et al. 1996a, b, Leite Ribeiro et al. 2012), field (De Serres et al. 1999) and numerical studies (Bradbrook et al. 1998, 2000, 2001, Biron et al. 2004, Đorđević & Biron 2008, Đorđević 2010, 2012, 2013). All laboratory data, except those of Biron et al. (1996a, b) and Leite Ribeiro et al. 2012, were collected in confluences of fixed-bed parallel channels. The data of Biron et al. are the only data from an asymmetrical fixed-bed Discordant Beds' (DB') confluence. As that was a single-flume confluence, the collected data carry the information on the combined effect of an upstream bend in the tributary and the bed elevation discordance. Additionally, the first 3D numerical models that were used to study the confluence hydrodynamics suffered from the numerical stability problems when modelling flow in dendritic domains (Bradbrook et al. 2001). Đorđević & Biron (2008) recently resolved the combined effect of the bed elevation discordance and the upstream bend was into separate contributions of the two controls using a 3D numerical model. Consequently, the role of bed elevation at the tributary entrance to the confluence was thoroughly studied in the 90° straight channels' confluence. Both the individual (Đorđević 2012, 2013) and the combined effect with an upstream bend (Đorđević 2013) were analysed. Moreover, in studying the combined effect of the two controls, different orientations of an upstream bend in the tributary were considered—case when the outer bank ends in the upstream junction corner (right bend) and that in which the outer bank ends in the downstream junction corner (left bend). The confluence with $\alpha = 90°$ was chosen as this junction angle allows development of all six regions in the CHZ recognised by Best (1988) (Fig. 1b).

The investigation of the role of the bed elevation discordance at the tributary entrance to the confluence was the first step towards the understanding of the complex flow phenomena in alluvial river

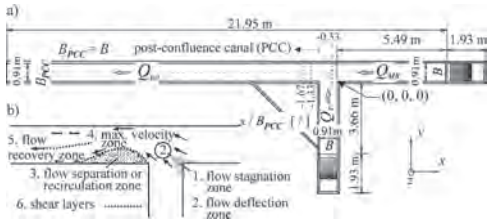

Figure 1. a) Plan view of the Shumate's laboratory canal (Shumate 1998), b) regions in the confluence hydrodynamics zone after Best (1988) (from Đorđević 2012).

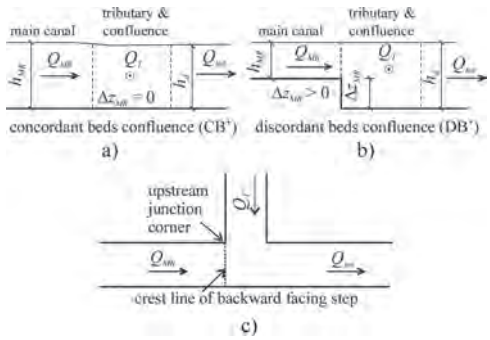

Figure 2. Definition sketch for the a) concordant and b) discordant beds' confluence layouts; c) position of the backward facing step in the main canal.

confluences. The second step is a study of effects of the bed elevation discordance in the Main River (MR). This study is performed in the present paper by using a 3D finite-volume based numerical model that was previously validated against Shumate's (1998) and Biron et al.'s (1996a, b) experimental data in Đorđević & Biron (2008), Đorđević (2010, 2012, 2013) and field data Đorđević (2010). Due to consistency with the previous studies, the confluence with the same planform and cross-sectional geometries is considered. Besides the Shumate's original layout (i.e. the concordant beds' confluence of two horizontal-bed canals with $\alpha = 90°$, sharp-edged corners and the width-to-depth ratio-$B/h \approx 3.0$), three hypothetical layouts, this time with the Δz_{MR} high backward facing step in the main canal, are analysed. Four values of the bed elevation discordance ratio ($\Delta z_{MR}/h_d$) in the range [0.0, 0.5] are considered. Here, Δz_{MR} stands for the difference in bed elevations between the upstream and downstream stretches of the main-canal and h_d for the flow depth in the main-canal at the confluence (Fig. 2b). The division of the main-canal is made at the upstream junction corner. The crest of the backward facing step, where the upstream stretch ends, is perpendicular to the main-canal axis (Fig. 2c). The value $\Delta z_{MR}/h_d = 0$ corresponds to the original Shumate's confluence layout and $\Delta z_{MR}/h_d = 0.50$ is the common value in river confluences (Biron et al. 1996b).

As in the previous studies, the role of the difference in bed elevations Δz_{MR} on the confluence hydrodynamics is assessed by the comparison of distributions of several variables. These are: 1) variations of flow angles at the tributary entrance to the confluence, 2) variations of the characteristic dimensions of the separation (or recirculation) zone (RZ) throughout the flow depth, 3) cross-sectional distributions of the stream-wise (u), lateral (v) and vertical (w) velocity components in the Post-Confluence Canal (PCC), 4) variations of the shear layer position and shear intensity throughout the flow depth and 5) non-dimensional bed shear stress distributions for the sand grain of size $d = 1$ mm. The consideration of all these aspects of confluence hydraulics is relevant for environmental and morphological studies, flood routing and bank protection in settlements situated at river confluences (Đorđević 2012).

2 SETUP OF NUMERICAL EXPERIMENTS

The present study is based on the geometry and the flow data (discharge combinations) from the Shumate's right-angled concordant beds' confluence of equal width canals (Fig. 1a). Three, out of six investigated discharge combinations, defined by the discharge ratio $D_R = Q_{MR}/Q_{tot}$ (Fig. 1a) are chosen for this study. These are $D_R = \{0.250, 0.583, 0.750\}$. The total discharge is the same in each experiment (0.17 m^3/s). The chosen discharge combinations cover a range of possible hydrological scenarios that might happen in a river confluence: 1) the dominance of the tributary flow ($D_R < 0.5$), 2) equal contributions of the combining flows ($D_R \approx 0.5$) and 3) the dominance of the main-river flow ($D_R > 0.5$). Numerical model, used in this study, was previously validated against the data from these experiments (Đorđević 2010, 2013, accepted).

The four considered confluence layouts are listed in Table 1. With three discharge combinations, this gives twelve different cases. In Discordant Beds' (DB') confluences, the main canal has an elevated, horizontal bed upstream of the confluence (i.e. there is a vertical backward facing step in the bed of the main-canal—Fig. 2b). The step is placed in line with the upstream junction corner (Fig. 2c).

The boundaries of the computational domain coincide with the boundaries of the Shumate's facility (Fig. 1a) to ensure no influence of the boundary conditions on the flow pattern in the CHZ.

Table 1. Grid size of the upstream part of block 1 for the considered confluence layouts.

Case no.	$\Delta z_{MR}/h_d$ [/]	Grid size of the upstream part of block 1	Description
1	0.00	$220 \times 38 \times 21$	Concordant beds' confl.
2	0.10	$220 \times 38 \times 19$	
3	0.25	$220 \times 38 \times 16$	Discordant beds' confl.
4	0.50	$220 \times 38 \times 11$	

3 NUMERICAL MODELLING

The 3D numerical model that was used in the previous studies (Đorđević & Biron 2008, Đorđević 2010, 2012, 2013) is also applied in this one. This is the SSIIM2 model (Olsen 2000), which solves Reynolds-averaged Navier-Stokes equations with the two-equation turbulence model closure. The system of equations is solved on an unstructured orthogonal/non-orthogonal multiblock grids. The SSIIM2 model is based on the finite-volume method. There are several two-equation models available in the SSIIM2. Due to consistency with the previous studies, the standard k-ε model is used in all numerical simulations in this paper. This choice is based on the fact that it showed the best performance during the model validation procedure. The mass and momentum equations are coupled using the SIMPLE algorithm. The convective terms in the momentum equations are discretised using the second-order upwind scheme as it provided better agreement with the experimental data (Đorđević 2010, 2013). The only option for presentation of the free-surface in SSIIM2 is the rigid-lid approach.

Since the flow in the Shumate's experiments was steady and subcritical, all numerical simulations are based on these two assumptions. Boundary conditions at solid boundaries are defined using the wall-law, while the zero-gradient condition is applied at the outflow boundary for the three velocity components (u, v, w), turbulence kinetic energy k and its dissipation rate ε. The vertical velocity component at the free-surface is calculated from the zero-discharge condition and the k is set to half of its bottom value. Constant discharges are prescribed at inflow boundaries and the constant depth is prescribed at the outflow boundary.

The computational domain consists of two orthogonal structured grids or blocks. Each canal of the Shumate's facility is covered with one block. The main canal is covered with the block 1 and the tributary canal with the block 2. The vertical size of block 1 upstream of the confluence varies with the change in the extent of the bed elevation discordance $\Delta z_{MR}/h_d$. The sizes of the block 2 and the part of the block 1 downstream of the upstream junction corner are the same in all confluence layouts. The size of block 2 is $183 \times 38 \times 21$ in the downstream, lateral and vertical directions, respectively. That of the downstream part of the block 1 is $658 \times 38 \times 21$. Grid sizes of the upstream part of the block 1 are given in Table 1 for the four considered confluence layouts.

4 RESULTS AND DISCUSSION

Before taking a long look at flow characteristics in the CHZ for different confluence layouts a general overview of flow patterns is given by presenting and discussing streamline plots on several horizontal planes above the canal bed (Fig. 3) and cross-sectional distributions of the three velocity components in the confluence and the post-confluence canal (Fig. 4).

It is readily noticeable that the presence of the Backward facing Step (BS) at the entrance of the upstream stretch of the main canal to the confluence helps the flow from the tributary to keep its original direction below the crest level (Fig. 3, cases 3 and 4 for $z/h_d = 0.10$). The portion of the tributary flow, which is affected by the presence of the BS, increases with the decreasing the dominance of the tributary flow ($D_R \geq 0.50$). Additionally, it increases with the increase in the step height (Fig. 3, see, for example, cases 2, 3 and 4 for $D_R = 0.750$).

The apparent "termination" of streamlines at the vertical step face (dashed line) and at the opposite wall means that the fluid moves vertically along these surfaces. Both the continuation of the tributary flow movement towards the opposite wall (bank) in the bottom layers ($z < \Delta z_{MR}$) and the consequent upward flow along the wall are visible on the cross-sectional distributions of the three velocity components (Fig. 4). The lateral velocity v at the bottom of the confluence cross-section $x/B_{PCC} = -0.333$ has 4–5 times greater magnitude than the stream-wise component u when $\Delta z_{MR} \geq 0.25 h_d$ (Figs. 1 and 4). Due to limited space u-velocity distribution is not presented in this cross-section. Moreover, the w-velocity reaches the same order of magnitude as $V_{xy} = (u^2 + v^2)^{1/2}$, the greatest magnitudes being attained for $D_R \approx 0.50$. The area of increased w-velocity magnitudes along the opposite wall extends 1.5–3 canal widths downstream of the BS, meaning that in the DB' confluences this bank not the one on the junction-side is endangered by erosion.

In the CB' confluence and DB' confluences with $\Delta z_{MR} \leq 0.25 h_d$ the $u_{\max}$ and the $u_{\max}$-core reduce as

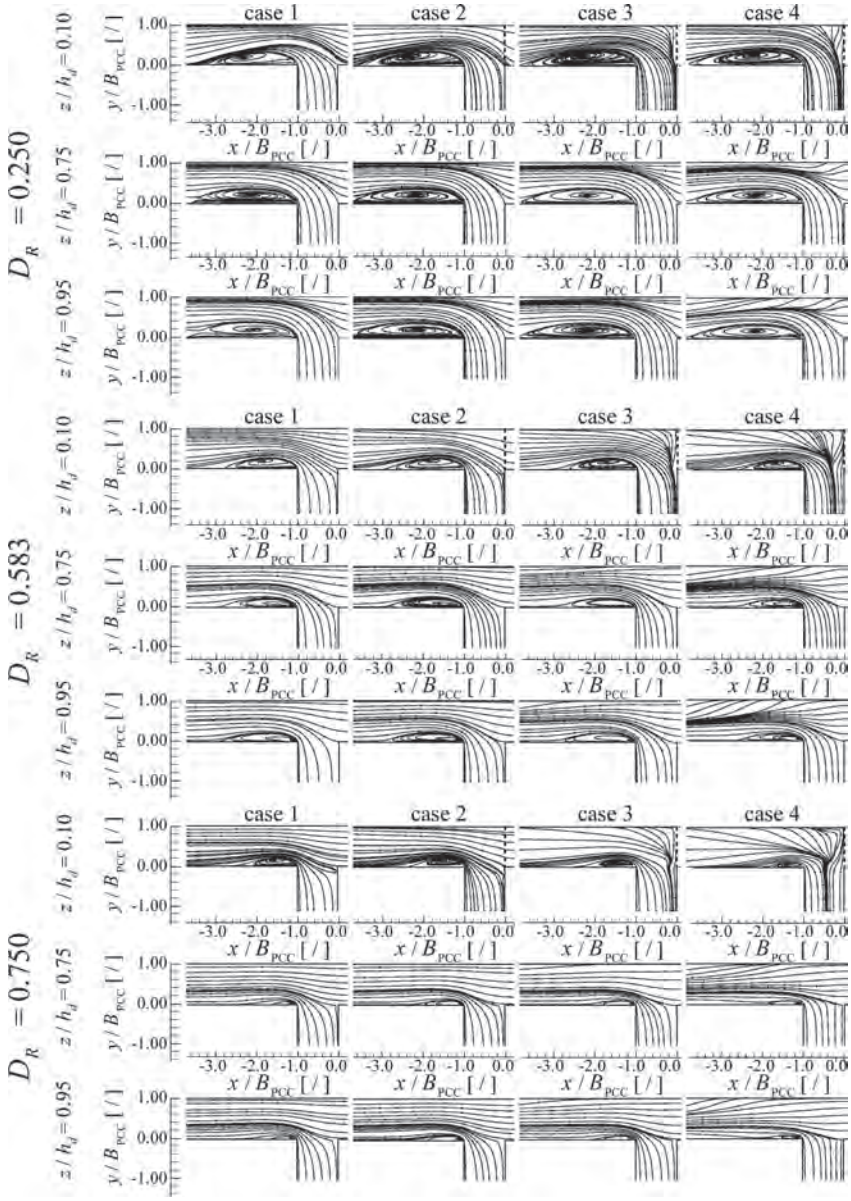

Figure 3. Streamlines on the horizontal planes at different non-dimensional elevations above the main-canal bed. Effects of D_R and $\Delta z_{MR}/h_d$ on the flow deflection at the tributary entrance to the confluence and on the size of the recirculation zone can be observed.

D_R increases (Fig. 4, cases 1, 2 and 3). In the DB' confluence with $\Delta z_{MR} = 0.50h_d$ the smallest u_{max} develops for $D_R = 0.583$ and the largest one for $D_R = 0.750$ (Fig. 4, case 4). Almost vertical isovels, which delineate the u_{max}-core when $D_R = 0.250$, deviate from the vertical when $D_R \geq 0.583$. The reduction of u-velocity magnitude along the opposite bank and pronounced deviation of the isovels on that side of the u_{max}-core are in line with the increase in the vertical velocity magnitude and the shape of upward w-velocity isovels (Fig. 4, case 4, u and w-velocity distributions).

One can also observe the change in the size of the Recirculation Zone (RZ) for different D_R and Δz_{MR}

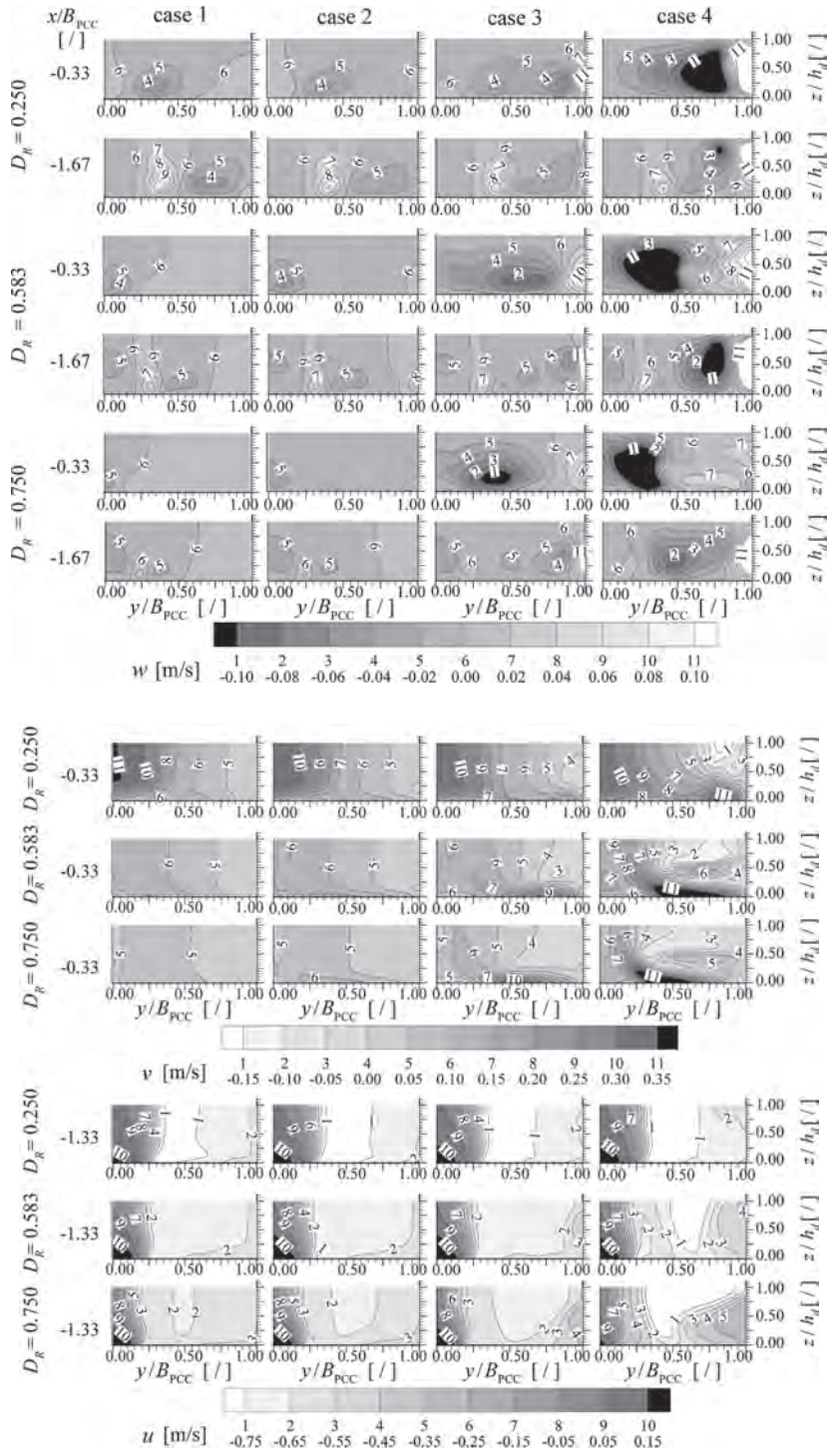

Figure 4. Effects of D_R and $\Delta z_{MR}/h_d$ on the cross-sectional distributions of the vertical (w), lateral (v) and stream-wise (u) velocities in the confluence and the post-confluence channel. **Note**: sign of the u-velocity follows from the accepted orientation of the coordinate system (Fig. 1a).

values on the cross-sectional u-velocity distributions (Fig. 4) and streamline plots (Fig. 3). The RZ length increases throughout the flow depth with the increase in Δz_{MR} when $D_R = 0.250$. However, it shortens for $D_R \geq 0.583$. The RZ width reduces with distance from the canal bed for the given confluence layout regardless the D_R-value. It is interesting to notice that the presence of the BS practically does not affect the RZ width for $D_R \leq 0.583$ and for $D_R = 0.750$ as long as $\Delta z_{MR} \leq 0.25 h_d$. Further increase in Δz_{MR} makes the RZ narrower.

A closer inspection of the flow characteristics in the CHZ starts at the entrance to the zone, i.e. in the flow deflection zone and continues with the RZ and the shear layer/layers. The study of the role of the bed elevation discordance Δz_{MR} in ends with the presentation of the bed shear stress distributions and the discussion about the possibilities for the initiation of motion of the sand grain of $d = 1$ mm.

Flow angles. Variations of flow angles δ (on the horizontal plane) and φ (on the vertical plane) at the tributary entrance to the confluence are presented in Figures 5 and 6, respectively. Results in Figure 5 confirm what was already noticed on the streamline plots in Figure 3, i.e. that the deflection of the tributary flow from the junction angle α is strongly affected by the presence of the BS in the main canal. It is readily noticeable that flow patterns differ for different D_R-values. The BS hardly affects δ-angle distributions when $D_R = 0.250$. The greatest discrepancies between the four cases exist near the bottom (Fig. 5, $D_R = 0.250$, $z/h_T = 0.008$). The shape of δ-lines remains essentially the same for $\Delta z_{MR} \leq 0.10 h_d$. Only the deflection from the α-angle reduces. No flow enters the tributary near

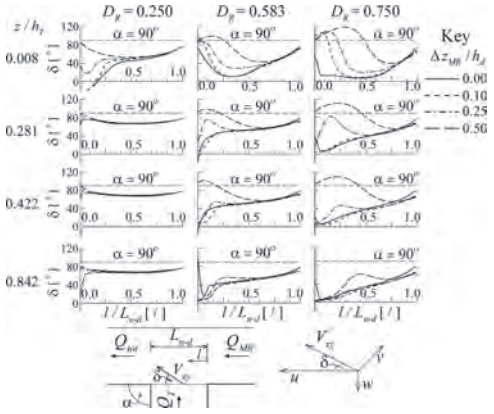

Figure 5. Effects of D_R and $\Delta z_{MR}/h_d$ on the δ-angle distributions at the tributary entrance to the confluence (z/h_T is the non-dimensional distance from the bottom of the tributary).

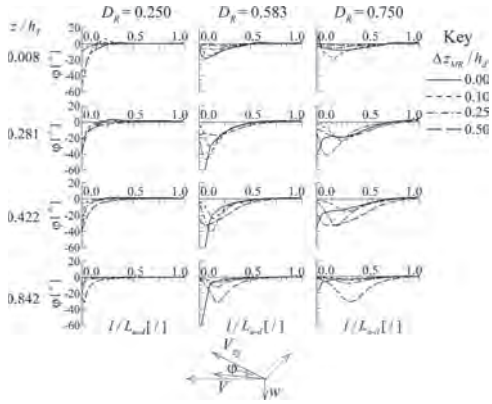

Figure 6. Effects of D_R and $\Delta z_{MR}/h_d$ on the φ-angle distributions at the tributary entrance to the confluence (z/h_T is the non-dimensional distance from the bottom of the tributary).

the upstream junction corner when $\Delta z_{MR} \geq 0.25 h_d$. Moreover, the flow continues forward in the same direction ($\delta \approx \alpha$) when $\Delta z_{MR} = 0.50 h_d$. Above $0.25 h_d$ the δ-angle is almost constant along $0.65 L_{u\text{-}d}$, i.e. its value varies in a narrow range—between 68° and 72°. However, for the BS as high as $0.50 h_d$, the tributary flow turns immediately at the upstream corner under the influence of the main-canal flow, which is comparably faster than that in the CB' confluence.

The δ-angle distributions become highly variable below the step-crest when $D_R \geq 0.583$ as Δz_{MR} increases.

Such a variation is a consequence of the pressure drop near the vertical step-face which causes redirection of one portion of the tributary flow upstream, towards the BS. The δ-angles of the redirected flow are greater than the junction angle ($\delta > \alpha$). The δ_{max} values are attained at $0.14 L_{u\text{-}d}$ near the bottom ($z/h_T = 0.008$) and at $0.08\ L_{u\text{-}d}$ for $z > 0.50 \Delta z_{MR}$. The corresponding minima are located approximately at $0.65 L_{u\text{-}d}$. The greatest portion of the tributary flow ($0.25 L_{u\text{-}d} = 0.25 B_T$) is redirected towards the BS when $D_R = 0.583$ (Fig. 5, $\Delta z_{MR} = 0.50 h_d$). The portion of the redirected flow reduces when approaching the crest level. The whole tributary flow turns downstream ($\delta < \alpha$) above $z = \Delta z_{MR}$ and δ-lines gradually become monotonously rising curves with the lowest δ-angle values (2°–3°) at the upstream junction corner where the two flows collide. Portions of the redirected tributary flow, the corresponding maxima and absolute values of minima are even greater when $D_R = 0.750$. It is also worth noting that δ-lines become almost linear above $0.70 h_d$ in DB' cases with $\Delta z_{MR} = 0.25 h_d$.

As far as the vertical flow deflection is concerned, it can be noticed from Figure 6 that the strongest 3D flow is confined to the upstream half of the junction-line regardless the confluence layout and the hydrological scenario. In this part of the cross-section the flow is always directed to the bottom (negative φ-angle values) due to its collision with the main-canal flow. The strong downward movement close to the upstream junction corner attenuates rapidly when $D_R = 0.250$. The presence of the bed-step higher than $0.25h_d$ attenuates vertical flow deflection in the bottom layers 4 to 7 times when compared to the CB' case.

However, from $z = 0.30h_d$ the absolute φ-angle value increases and becomes 4.5 times larger than the bottom value at $z = \Delta z_{MR}$. The $|\varphi_{min}|$ decreases gradually above the step-crest. The absolute minimum moves from the upstream towards the downstream junction corner with the increase in D_R giving the δ-lines shape of a parabola in contrast to the CB' case. This shape is preserved throughout the flow depth in DB' confluences, while in the CB' confluence it turns to hyperbola again by $z = 0.10h_d$. The absolute maximum $|\varphi_{min}|$ is reached around $z = \Delta z_{MR}$ within $0.20L_{u\text{-}d}$. In the upper layers φ-peaks move downstream, but never farther than $0.36L_{u\text{-}d}$. The angle changes its sign (becomes positive) between 0.50 and 0.90 $L_{u\text{-}d}$ depending on the Δz_{MR}-value. However, these values are very low when compared to the negative ones, meaning that the 3D flow is practically suppressed at the downstream junction corner.

Recirculation zone. Variations of the RZ length and its maximal width are presented in Figure 7. Unlike the presence of the bed-step at the tributary entrance to the confluence (Đorđević 2012, 2013), the corresponding one in the main canal allows development of the RZ throughout the flow depth. The largest zone develops when $D_R = 0.250$ regardless the confluence layout. The greatest extensions of the RZ length are close to the bottom (20–40% depending on Δz_{MR}). They reduce towards the free-surface, but never drop below 13%. Contrary to the CB' confluence, the RZ width is almost constant throughout the flow depth. The influence of the bed-step on the RZ length is practically negligible when $D_R \geq 0.583$ as long as $\Delta z_{MR} \leq 0.25h_d$ (1–7% depending on D_R-value). However, for $\Delta z_{MR} = 0.50h_d$ and $D_R = 0.583$, the zone is systematically shortened and narrowed by 20% throughout the flow depth, which means that the shape of the zone remains unaltered. This is not the case when $D_R = 0.750$ (40% reduced RZ length gradually increases towards the free-surface where it equates with that in the CB' case).

The observed regularity for the RZ length does not hold for its width when $D_R = 0.583$. For this D_R-value only the bed-step with $\Delta z_{MR} = 0.25h_d$ has no effect on the RZ width. The regularity re-establishes for $D_R = 0.750$.

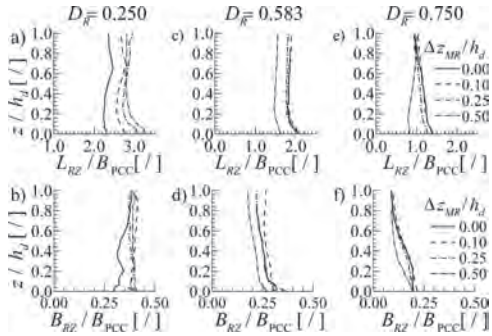

Figure 7. Effects of D_R and $\Delta z_{MR}/h_d$ on the size of recirculation zone. First row presents variations of non-dimensional RZ length, and the second one, variations of the non-dimensional RZ width throughout the flow depth.

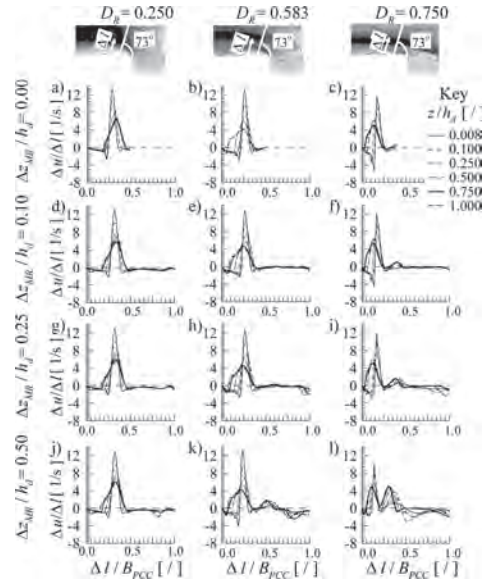

Figure 8. Effects of D_R and $\Delta z_{MR}/h_d$ on the shear layer position and shear intensity. Shear distributions are drawn at several elevations above the canal bed along arbitrary lines indicated on the top plates.

Shear layer. The position and the shape of the shear layer can be traced on the cross-sectional *u*-velocity distributions (Fig. 4). To facilitate comparison between the twelve cases, shear distributions are drawn along arbitrary lines presented in the top row in Figure 8. Generally, the greatest shear is developed near the bottom, and the smallest one near the free-surface. The shear intensity reduces with the increase in D_R when $\Delta z_{MR} \leq 0.25h_d$.

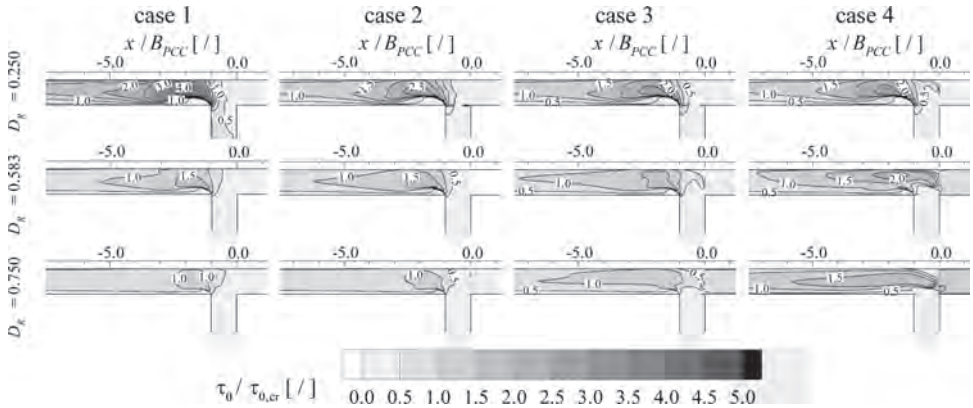

Figure 9. Non-dimensional bed shear stress distributions for the sand grain of 1 mm size.

However, in the DB' confluence with $\Delta z_{MR} = 0.50h_d$ the greatest shear develops for $D_R = 0.583$. It is interesting to notice that two shear layers, one on each side of the u_{max}-core, exist in DB' confluences when $D_R = 0.750$. The shear intensity between the RZ and u_{max}-core is greater than the one on the opposite side. The only exception is the confluence with $\Delta z_{MR} = 0.50h_d$ where the intensity is equal in both shear layers. Moreover, in this type of confluence two layers with unequal shear intensities also develop when $D_R = 0.583$.

Bed shear stress distributions are presented in Figure 9. They are non-dimensionalised with the critical shear stress for the sand grain of 1 mm size. The effect of the bed-step differs for the scenarios with $D_R = 0.250$ and for $D_R \geq 0.583$. In the former one, the presence of the bed-step reduces both the $\tau_{0,max}$ and the area with maximal τ_0-values, while in the latter one it provides conditions for the sand grain movement far downstream of the confluence ($> 5B_{PCC}$). The percentage reductions for $\tau_{0,max}$ are approximately the same (38%) in all confluence layouts when $D_R = 0.250$. Those for the length of the area with $\tau_0/\tau_{0,cr} \geq 2.5$ are 47% for $\Delta z_{MR} = 0.10h_d$ and 51% for $\Delta z_{MR} \geq 0.25h_d$. On the other hand, the area with possible movement of 1 mm sand grain is extended, depending on the D_R-value, 1.1 to 7 times when compared to that in the CB' case.

5 CONCLUSIONS

A 3D finite-volume based numerical model SSIIM2 was used to study the role of bed elevation discordance in the main-river on the confluence hydrodynamics. Three characteristic hydrological scenarios were analysed in 90º straight-channels' confluences having four different riverbed geometries They include cases that range between the confluence with no difference in bed elevations and the confluence with the maximal observed value of bed elevation discordance ratio in alluvial rivers. The following conclusions are derived from this study.

1. The pressure drop caused by the difference in bed elevations at the entrance of the upstream stretch of the main canal to the confluence gives rise to the division of the tributary flow at elevations below the bed of the shallower canal. The flow is divided into the part that which turns upstream towards the bed-step face and that which turns downstream to enter the PCC.
2. The portion of the tributary flow affected by the pressure drop increases with the increase in both the bed elevation discordance ratio and the dominance of the main-canal flow.
3. The existence of the bed elevation discordance in the main-river enhances 3D flow in: 1) the upper layers ($z > \Delta z_{MR}$) at the tributary entrance to the confluence, 2) the confluence and 3) the PCC.
4. The vertical velocity (w) reaches the same order of magnitude as the horizontal velocity V_{xy} in DB' confluences with high $\Delta z_{MR}/h_d$ values (≥ 0.25). As opposed to the CB' confluence, very large upward velocities are developed along the opposite wall meaning that this bank, not the one on the junction-side, is endangered by erosion.
5. The bed elevation difference Δz_{MR} has the adverse effect on the RZ size when $D_R = 0.250$ and $D_R \geq 0.583$. It promotes extension and widening of the RZ for $D_R = 0.250$. The RZ growth follows the Δz_{MR} rise, i.e. the largest RZ is developed for $\Delta z_{MR} = 0.50h_d$. The effect of Δz_{MR} on the RZ length is practically negligible up to $\Delta z_{MR} = 0.25h_d$ for $D_R \geq 0.583$. In the DB' confluences with $\Delta z_{MR} = 0.50h_d$ the shape of the

RZ is preserved when $D_R = 0.583$, but the zone is reduced by approximately 20%. With further increase in the D_R-value the RZ is shortened in the bottom $0.70h_d$ and narrowed between 0.20 and 0.80 h_d.

6. The shape of the u_{max}-core is markedly distorted due to enhanced 3D flow in DB' confluences with $\Delta z_{MR} \geq 0.25h_d$ when $D_R \geq 0.583$. The distortion gives rise to the development of the secondary shear layer in the upper half of the water column on the side of the core towards the opposite wall in addition to the primary one, which develops between the RZ and the maximal velocity zone. The shear intensity in the secondary shear layer is 3 to 5 times lower than that in the primary one. However, shear intensities in the two layers become almost equal when $\Delta z_{MR} = 0.50h_d$ and $D_R = 0.750$.
7. The size of the area with maximal bed-shear stress ($\tau_{0\ max}$) on the canal bottom does not change in DB' confluences when $D_R = 0.250$. However, the $\tau_{0\ max}$ reduces by ≈ 38% regardless the Δz_{MR}-value. When $D_R \geq 0.583$ the bed elevation discordance favours conditions for the movement of 1 mm sand grains both in the confluence and the PCC. The greater the Δz_{MR} is, the farther the area with $\tau_0/\tau_{0,cr} > 1$ extends.

REFERENCES

Ashmore, P. & Parker, G. 1983. Confluence scour in coarse braided streams. *Water Resour. Res*. 19(2): 392–402.

Best, J.L. 1988. Sediment transport and bed morphology at river channel confluences. *Sedimentology* 35: 481–498.

Best, J.L. & Roy, A.G. 1991. Mixing-layer distortion at the confluence of channels of different depth. *Nature* 350: 411–413.

Biron, P., Roy, A.G. & Best, J.L. 1996a. Turbulent flow struc-ture at concordant and discordant open-channel con-fluences, *Experiments in Fluids* 21: 437–446.

Biron, P., Best, J.L. & Roy, A.G. 1996b. Effects of bed discordance on flow dynamics at open-channel confluences. *J. Hydraul. Eng.* ASCE, 122(12): 676–682.

Bradbrook, K.F., Biron, P., Lane, S.N., Richards, K.S. & Roy, A.G. 1998. Investigation of controls on secondary circulation in a simple confluence geometry using a three-dimensional numerical model, *Hydrological Processes* 12: 1371–1396.

Bradbrook, K.F., Lane, S.N. & Richards, K.S. 2000. Numerical simulation of the three-dimensional, time-averaged flow structure at river channel confluences. *Water Resour. Res.* 36(9): 2731–2746.

Bradbrook, K.F., Lane, S.N., Richards, K.S., Biron, P.M. & Roy, A.G. 2001. Role of bed discordance at asymmetrical river confluences. *J. Hydraul. Eng*. ASCE, 127(5): 351–368.

De Serres, B., Roy, A.G., Biron, P.M. & Best, J.L., 1999. Three-dimensional structure of flow at a confluence of river channels with discordant beds, *Geomorphology*, 26: 313–335.

Đorđević, D. & Biron, P.M., 2008. Role of upstream planform curvature at asymmetrical confluences—laboratory exp-eriment revisited. *Proc. 4th Int. Conference on Fluvial Hyd-raulics—River Flow 2008, Cesme* 3: 2277–2286.

Đorđević, D. 2010. *Numerical investigation of the river confluence hydrodynamics.* Unpublished PhD Dissertation, University of Belgrade, Belgrade, 382p.

Đorđević, D. 2012. Role of bed elevation discordance at 90º straight channel confluences. *Proc. Int. Conference on Fluvial Hydraulics—River Flow 2012, San Hose,* 3: 2277–2286.

Đorđević, D. 2013. Numerical study of 3D flow at right-angled confluences with and without upstream planform curvature. *J. of Hydroinformatics,* 15.4: 1073–1088.

Đorđević, D. (accepted). Can a 3D-numerical model be a substitute to a physical model in estimating parameters of 1D-confluence models?. (submitted to 3rd IAHR-Europe Congress).

Gaudet, J.M. & Roy, A.G., 1995. Effect of bed morphology on flow mixing length at river confluences. *Nature* 373: 138–139.

Kennedy, B. 1984. On Playfair's law of accordant junctions. *Earth Surface Processes and Lanforms,* 9: 153–173.

Leite Ribeiro, M., Blankaert, K., Roy, A.G. & Schleiss, A.J. 2012. Flow and sediment dynamics in channel confluences. *J. Geophys. Res.*, 117, F01035, DOI: 10.1029/2011JF002171.

Mosley, M.P. 1976. An experimental study of channel con-fluences. *Journal of Geology* 94: 535–562.

Olsen, N.R. 2000. *CFD Algorithms for Hydraulic Engineering*. Trondheim: The Norwegian University of Science and Technology.

Shumate, E.D., 1998. *Experimental description of flow at an open-channel junction.* Unpublished Master thesis, Univ. of Iowa, Iowa, 150 p.

Weerakoon, S.B., Tamai, N. & Kawahara, Y. 1990. Bed topography, bed shear stress distribution and velocity field in a confluence. *Proc. of Hydraulic Engineering, JSCE,* 34: 307–312.